



Since January 2020 Elsevier has created a COVID-19 resource centre with free information in English and Mandarin on the novel coronavirus COVID-19. The COVID-19 resource centre is hosted on Elsevier Connect, the company's public news and information website.

Elsevier hereby grants permission to make all its COVID-19-related research that is available on the COVID-19 resource centre - including this research content - immediately available in PubMed Central and other publicly funded repositories, such as the WHO COVID database with rights for unrestricted research re-use and analyses in any form or by any means with acknowledgement of the original source. These permissions are granted for free by Elsevier for as long as the COVID-19 resource centre remains active.

It's Not All in Your Head: Thoracic Manifestations of Neurologic Diseases and Disorders

Girish S. Shroff, MD, Carol C. Wu, MD, Daniel Ocazonez, MD, Brett W. Carter, MD, Akhil Shivaprasad, MBBS, Thomas Chai, MD, Emilio P. Supsupin, MD, Mylene T. Truong, MD, Sheetal Shroff, MBBS

Myriad conditions may affect both the neurologic system and the thorax, while other diseases primarily affecting the thorax may manifest with neurologic abnormalities. Correlation of signs, symptoms, and imaging findings in the neurological system with those in the thorax can help diagnose certain conditions and/or guide further diagnostic work-up and treatment. We will review and illustrate the imaging appearance of several systemic/neurological diseases with thoracic manifestations as well as discuss conditions in the thorax that can lead to neurologic symptoms.

© 2020 The Association of University Radiologists. Published by Elsevier Inc. All rights reserved.

INTRODUCTION

A variety of conditions, including inflammatory, infectious, malignant, vascular, and congenital processes, can affect both the neurologic system and the thorax. Other diseases presenting initially in the thorax may initially present with or later manifest neurologic abnormalities. Correlation of signs, symptoms, and imaging findings in the nervous system with those in the thorax can help diagnose certain conditions and/or guide further diagnostic evaluation and therapy. In this article, we will review the clinical manifestations and imaging findings of conditions that involve both the neurologic system and the thorax, with emphasis on several of the lesser known entities.

INFLAMMATORY CONDITIONS

IgG4-related Disease (IgG4-RD)

Immunoglobulin G4-related disease (IgG4-RD) is a fibroinflammatory disease of unknown etiology characterized by tumefactive lesions in one or more organs, a lymphoplasmacytic infiltrate rich in IgG4-positive plasma cells and associated fibrosis, and often, elevated serum IgG4 concentrations (1,2).

Lymphoma is the closest histopathological mimicker of IgG4-RD (2). Comprehensive diagnostic criteria for IgG4-RD have been established (1) and will not be detailed here though it should be noted that IgG4-positive plasma cells can be detected in other inflammatory diseases, and elevated serum IgG4 concentration is common in, though not specific for, IgG4-RD (3). The pancreas is the most commonly affected organ but any organ system can be involved and clinical symptoms are dependent upon the organs involved. Serious complications can result from obstructive or compressive symptoms related to organomegaly, and organ failure can result from cellular infiltration or fibrosis (1). Of note, many previously recognized conditions are now acknowledged to fall in the spectrum of IgG4-RD, including Riedel's thyroiditis, inflammatory pseudotumor, and mediastinal and retroperitoneal fibrosis (2).

Lymphadenopathy, found in 53% of patients with intrathoracic IgG4-RD, was the most common intrathoracic manifestation of IgG4-RD in a review of 87 patients with intrathoracic IgG4-RD (4). In terms of pulmonary findings, 4 major types of IgG4-related lung manifestations have been defined by Inoue et al.: (1) solid nodule or mass (Fig 1A), (2) multiple rounded ground-glass opacities, (3) alveolar interstitial (i.e., diffuse ground-glass opacities, bronchiectasis, and honeycombing), and (4) bronchovascular disease (i.e., thickening of bronchovascular bundles and interlobular septa) (5). Signs and symptoms of IgG4-related lung disease include cough, fever, dyspnea on exertion, and chest pain; patients may be asymptomatic (5). Pleural manifestations of IgG4-RD include nodules/thickening and effusion (4). Cardiovascular involvement in IgG4-RD includes aortitis-periaortitis (Fig 1B), large-medium vessel arteritis-periarthritis, and inflammatory

Acad Radiol 2020; ■:1-12

From the MD Anderson Cancer Center, 1515 Holcombe Blvd. Unit 1478, Houston, TX (G.S.S., C.C.W., B.W.C., T.C., M.T.T.); UT Health Science Center at Houston, Houston, TX (D.O., E.P.S.); Houston Methodist, Houston, TX (A.S., S.S.). Received May 21, 2020; revised June 11, 2020; accepted June 12, 2020. Address correspondence to: G.S.S. e-mail: gshroff@mdanderson.org

© 2020 The Association of University Radiologists. Published by Elsevier Inc. All rights reserved.

<https://doi.org/10.1016/j.acra.2020.06.017>

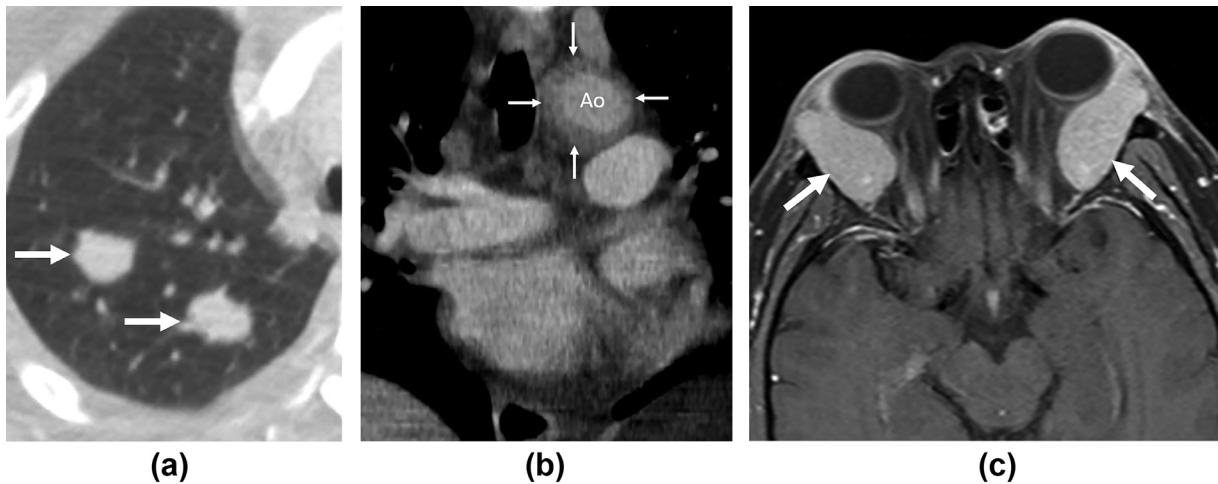


Figure 1. IgG4-related disease (IgG4-RD).

A and B, A 49-year-old woman for pulmonary nodule evaluation. A, Contrast-enhanced chest CT (lung windows) shows several nodules in the right lung (arrows). B, Contrast-enhanced coronal CT reformation depicts circumferential thickening of the wall of the aortic arch (arrows). Pulmonary nodule biopsy revealed IgG4-RD. Aortic wall thickening was presumed to represent IgG4-related aortitis. Ao, aorta. Lymphadenopathy is the most common intrathoracic manifestation of IgG4-RD but the lungs, pleura, and vascular system can also be involved.

C, A 35-year-old woman with exophthalmos. Contrast-enhanced MRI shows diffuse enlargement and enhancement of both lacrimal glands (arrows). Lacrimal gland biopsy showed IgG4-RD (i.e., IgG4-related dacryoadenitis). Neurological manifestations of IgG4-RD result primarily from orbital, pachymeningeal (i.e., dural), and pituitary involvement.

aneurysms (6). Yabusaki et al. found that the most common site of IgG4-related vasculitis was the iliac arteries (35%), followed by the infrarenal aorta (33%), thoracic aorta and first branches of the thoracic aorta (8%), suprarenal abdominal aorta (6%), and first branches of the abdominal aorta (5%) (7). The coronary arteries (arteritis and aneurysms) and pericardium can also be involved (6).

Neurological manifestations of IgG4-RD result primarily from orbital/ophthalmic involvement, pachymeningeal (i.e., dural) disease, and hypophyseal (i.e., pituitary gland and stalk) disease (8). IgG4-related orbital disease, of which lacrimal gland involvement (dacryoadenitis) is the most common manifestation (Fig 1C), is typically bilateral, painless, and has an insidious onset (8,9). Other orbital contents that can be involved by IgG4-RD include the extraocular muscles and intraorbital nerves, including the optic nerve (8). Dacryoadenitis in conjunction with parotid and submandibular gland enlargement (a triad formerly known as Mikulicz' disease) has a high positive predictive value for the diagnosis of IgG4-RD (8). Pachymeningitis can present with symptoms related to mechanical compression of structures (e.g., cranial palsies) or with more generalized symptoms such as headache, seizures, or cognitive decline (10). Both IgG4-related pachymeningitis and IgG4-related hypophysitis occur more commonly as a single-organ manifestation of disease rather than in the context of multiorgan involvement (8).

Wallace et al. have identified 4 distinctive IgG4-RD phenotypes according to organ involvement: (1) Pancreato-hepato-biliary disease, (2) retroperitoneal fibrosis and/or aortitis, (3) head and neck-limited disease, and (4) classic Mikulicz syndrome with systemic involvement (11). The frequency of association between thoracic and neurological manifestations remains to be elucidated.

DERMATOMYOSITIS/POLYMYOSITIS

Dermatomyositis (DM) and polymyositis (PM) are idiopathic inflammatory myopathies characterized by symmetric proximal muscle weakness and muscle inflammation (12). DM affects women more than men and children can also be affected whereas PM rarely affects children (12). DM, unlike PM, is associated with characteristic skin eruptions (including a heliotrope rash on the upper eyelids and Gottron's papules on the dorsal aspects of the metacarpophalangeal and interphalangeal joints) that can accompany or precede muscle weakness (12). Interstitial lung disease (ILD) is reported to occur in 5-30% of DM-PM patients (13). ILD patterns associated with DM-PM include nonspecific interstitial pneumonia (NSIP, most common), organizing pneumonia (OP), usual interstitial pneumonia (UIP), and diffuse alveolar damage (DAD) (13). Importantly, both DM and PM (but particularly DM) are associated with an increased risk of malignancies, of which lung cancer is the most common (14) (Fig 2A). Newly diagnosed DM-PM patients therefore usually undergo cancer screening (15). When associated with an underlying malignancy, DM (or PM) is considered a paraneoplastic syndrome (Figs 2B and 2C). In these cases, treatment of the malignancy generally results in regression of DM; similarly, recurrence of DM can herald recurrence of malignancy (16).

SARCOIDOSIS

Characterized by the presence of noncaseating granulomata, sarcoidosis is a multisystem granulomatous disease of unknown etiology. It is three times more common in black Americans than in white Americans and usually develops

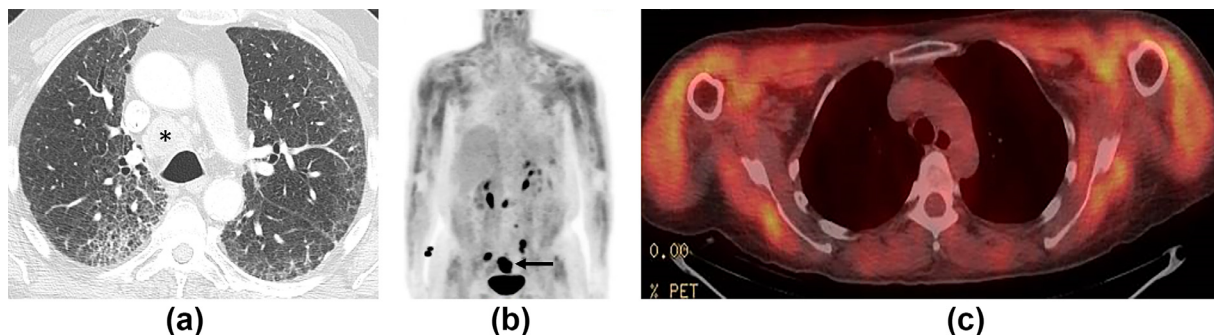


Figure 2. Polymyositis (PM)-Dermatomyositis (DM).

A, A 69-year-old man with polymyositis. Contrast-enhanced chest CT shows subpleural predominant interstitial lung disease, biopsy proven nonspecific interstitial pneumonitis (NSIP). Biopsy of the 2.8 cm right paratracheal node (*) revealed metastatic lung adenocarcinoma. Both dermatomyositis and polymyositis are associated with an increased risk of a variety of malignancies, of which lung cancer is the most common.

B and C, A 65-year-old woman with endometrial carcinoma, recently diagnosed with dermatomyositis as a paraneoplastic syndrome. Whole-body PET (B) and axial fused PET/CT (C) show diffuse intramuscular uptake of radiotracer, most notable in the proximal upper extremities, consistent with dermatomyositis. Arrow in B denotes the endometrial malignancy. When associated with an underlying malignancy, dermatomyositis and polymyositis are considered paraneoplastic syndromes. (Color version of figure is available online.)

before the age of 50 (peak incidence at age 20–39) (17). The lungs and intrathoracic nodes are most commonly affected but any organ system can be involved. Systemic symptoms (e. g., fatigue, night sweats and weight loss) are common (17). Respiratory symptoms include dyspnea and cough. Patients are frequently asymptomatic. On chest CT, sarcoidosis is characterized by symmetric bilateral hilar and mediastinal adenopathy and pulmonary nodules that predominate in the upper lobes and peribronchovascular and subpleural regions (Fig 3A). Lung nodules can conglomerate into larger nodules and even masses, termed progressive massive fibrosis. Lung abnormalities may progress to fibrosis. Neurologic symptoms due to central nervous system (CNS) involvement occur in ~5% of sarcoid patients – cranial nerve deficits, headache, and seizures are most common (18). Neurosarcoidosis has a predilection for the leptomeninges, especially the basilar meninges, and leptomeningeal disease is seen in ~40% of neurosarcoidosis cases (19) (Fig 3B). Other sites of neurologic involvement include the cranial nerves, brain, spinal cord, nerve roots, dura, and bone (19).

INFECTIOUS CONDITIONS

COVID-19

COVID-19 (coronavirus disease 2019) refers to disease caused by severe acute respiratory syndrome coronavirus 2 (SARS-CoV-2), a novel coronavirus identified as the cause of a cluster of cases of pneumonia in Wuhan, China in December 2019. The disease spread rapidly and was declared a Public Health Emergency of International Concern by the World Health Organization (WHO) on January 30, 2020 and a pandemic on March 11, 2020 (20). As of May 19, 2020, over 4.9 million cases and over 320,000 deaths have been reported worldwide (21). Common symptoms at illness onset include fever, fatigue, and dry cough; pneumonia is the

most frequent serious manifestation (22). On CT, COVID-19 pneumonia typically presents with bilateral ground-glass opacities +/- consolidation in a peripheral or posterior distribution, often with lower lobe predominance (23–27) (Fig 4A). As disease progresses, consolidation, greater total lung involvement, linear opacities, the “crazy-paving” pattern, and the reverse halo sign can be seen (25,28). Pneumonia can lead to acute respiratory distress syndrome (ARDS). Importantly, chest CT can be normal in the early stage of infection (i.e., 0–2 days after symptom onset) (28). Less typical manifestations of COVID-19 include gastrointestinal and neurologic symptoms (22). In a review of 214 hospitalized patients with confirmed infection in Wuhan, neurologic manifestations were seen in 36.4% and were categorized as: (1) CNS (dizziness, headache, impaired consciousness, stroke, ataxia, seizure), (2) peripheral nervous system (impairment of taste, smell, vision, and nerve pain) and (3) skeletal muscle (29). Oxley et al. recently reported that large-vessel ischemic stroke was a presenting feature of COVID-19 in five patients younger than age 50 (30) (Fig 4B). Encephalopathy (31,32), including acute necrotizing hemorrhagic encephalopathy, (33) and Guillain-Barre syndrome (34) have also been reported.

Invasive Aspergillosis (IA)

Aspergillus organisms are part of the normal environmental flora in the soil. Humans are therefore routinely exposed to Aspergillus organisms, however, aspergillus infection is uncommon (35). Invasive aspergillosis (IA), the most severe form of infection with Aspergillus, is a disease of highly immunocompromised patients. At-risk patients include those with prolonged neutropenia, hematopoietic stem cell and solid organ transplant recipients, and patients with advanced acquired immunodeficiency syndrome (AIDS) or chronic granulomatous disease (35). Because inhalation is the most

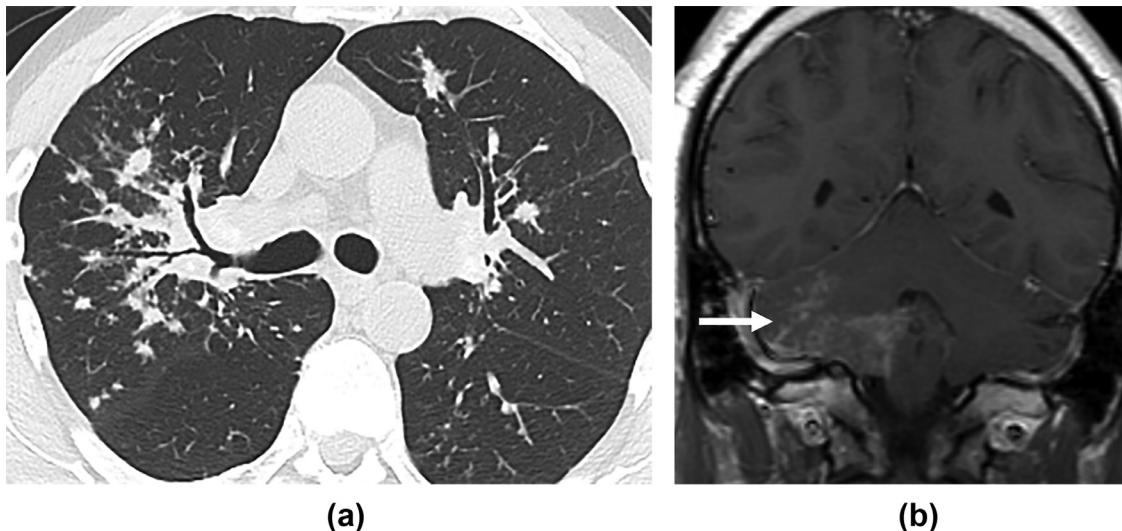


Figure 3. Sarcoidosis.

A, A 67-year-old man with pulmonary sarcoidosis. Noncontrast chest CT (lung windows) shows characteristic bilateral peribronchovascular nodularity.

B, A 36-year-old black man with headache and blurred vision. Coronal T1-weighted contrast-enhanced brain MRI shows leptomeningeal enhancement in the right cerebellum (arrow), biopsy proven neurosarcoidosis. Neurologic symptoms due to CNS involvement occur in ~5% of patients with sarcoidosis.

common route of entry for aspergillus spores, IA principally involves the sinopulmonary tract, and the lungs are the most common site of infection (35). Fever, cough, and dyspnea are frequent presenting symptoms of lung infection.

Invasive infection is most commonly caused by *Aspergillus fumigatus*. Characterized by tissue invasion, IA may be divided into airway-invasive aspergillosis (~10% of cases of IA) and angioinvasive aspergillosis (AIA). AIA is characterized histologically by the invasion and occlusion of small to medium pulmonary arteries by fungal hyphae and subsequent hemorrhagic infarction (36). On chest CT, hemorrhagic infarction

caused by AIA characteristically manifests with the halo sign, a solid nodular opacity surrounded by a halo of ground glass (Fig 5A). In neutropenic patients, the halo sign (though not specific for AIA) is highly suggestive of AIA. Considered an early sign in AIA infection, the halo sign is seen in greater than 90% of patients at presentation but only in ~20% at day 7 (37,38). In contrast, the air-crescent sign, a crescent-shaped lucency within a nodule or area of consolidation, is not typically seen at presentation but rather later in the course of the disease (~60% of patients at day 14) and is thought to be an indicator that the infection is improving (37). In immunosuppressed patients, invasive fungal infection can manifest as the reversed halo sign, a focal round ground-glass opacity surrounded by a crescent or ring of consolidation. The angioinvasive nature of the infection allows *Aspergillus* organisms to disseminate beyond the lungs to any organ system. A potential devastating consequence of infection, dissemination to the CNS can lead to seizures or focal neurologic signs from mass effect or stroke (35) (Fig 5B).

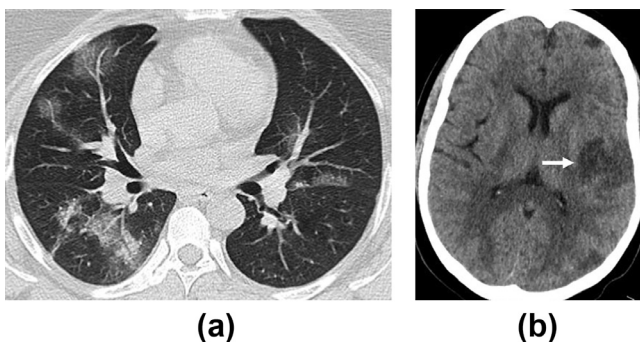


Figure 4. COVID-19.

A, A 39-year-old woman with COVID-19. Noncontrast chest CT (lung windows) shows bilateral peripheral ground-glass opacities in the lungs characteristic for COVID-19 pneumonia.

B, Brain CT performed 1 week after admission when the patient developed right-sided weakness and facial droop shows a left middle cerebral artery territory infarct (arrow). Ischemic stroke is a potential complication of COVID-19 and may be a presenting feature of disease in younger patients.

Tuberculosis (TB)

TB infection, caused usually by *Mycobacterium tuberculosis*, is classified as pulmonary, extrapulmonary, or both (39). Pulmonary TB has conventionally been categorized as primary or reactivation/postprimary, however, evidence from TB-endemic areas indicates that a substantial percentage of active TB infections in adults are the result of recent infection (either primary infection or reinfection with a new strain) and not reactivation (39,40). Primary TB, which develops soon after initial infection, is seen typically in children and immunocompromised patients, and manifests with

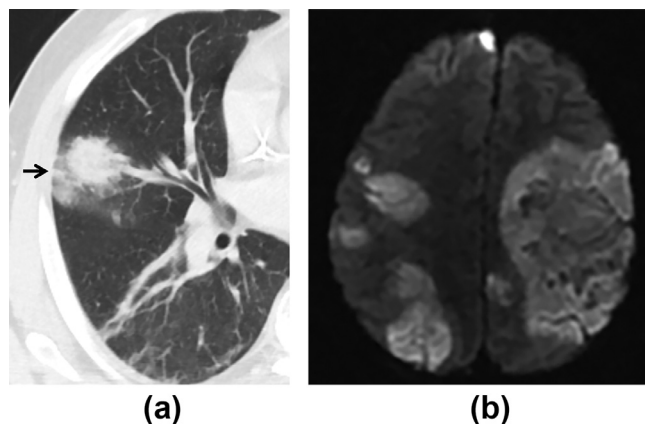


Figure 5. Invasive Aspergillosis

A, A 35-year-old man with myelodysplastic syndrome and neutropenic fever. Noncontrast chest CT (lung windows) shows the halo sign, a solid nodule partially surrounded by a halo of ground-glass attenuation (*arrow*). In immunocompromised patients, the halo sign is highly suggestive of angioinvasive aspergillosis.

B, Diffusion-weighted brain MR performed for acute neurologic deterioration shows multiple infarcts in different vascular territories. Autopsy revealed *Aspergillus* hyphae in the brain parenchyma. The angioinvasive nature of *Aspergillus* infection allows hematogenous dissemination from the lungs to any organ system.

adenopathy, consolidation, and pleural effusion (41). Postprimary TB (the result of either reactivation of endogenous, primary infection or recent exogenous infection) (42) characteristically manifests with cavitation, patchy consolidation, and centrilobular nodules (41) (Fig 6A). Imaging features of primary TB and reactivation TB are often similar and integrity of host immune response may be the only independent predictor of imaging appearance; severely immunocompromised patients tend to have the primary form, whereas immunocompetent patients tend to have the reactivation

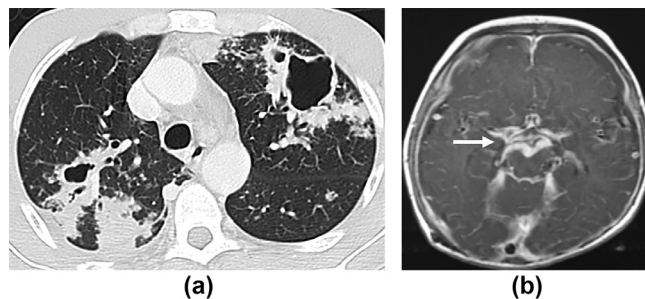


Figure 6. Tuberculosis.

A, A 35-year-old man with pulmonary tuberculosis. Contrast-enhanced chest CT shows cavitory and consolidative opacities in bilateral upper lobes.

B, A 15-year-old girl with nuchal rigidity. Contrast-enhanced brain MRI shows thick enhancement at the basal cisterns/basal meninges (*arrow*). Cerebrospinal fluid analysis revealed tuberculous meningitis. Tuberculous meningitis is the most common CNS manifestation of TB.

form (43,44). Miliary disease can occur in primary or postprimary TB and results from hematogenous dissemination. Cavitory disease can lead to Rasmussen aneurysm, a pseudoaneurysm that results from weakening of the pulmonary artery wall by adjacent cavitory disease (43). CNS involvement is seen in ~5% of patients with TB though prevalence is greater in immunocompromised patients (45). Usually the result of hematogenous spread, CNS TB may also result from direct rupture or extension of a subependymal or subpial focus (45). Tuberculous meningitis is the most common CNS finding of TB (Fig 6B); other manifestations include tuberculoma, abscess, cerebritis, and miliary disease (45).

MALIGNANCIES AND CONDITIONS ASSOCIATED WITH MALIGNANCY

Paragangliomas

Paragangliomas, including pheochromocytomas, are tumors that arise from autonomic paraganglia. Paraganglia are neuroendocrine cells found in several locations in the body; some are associated with the sympathetic nervous system, others with the parasympathetic nervous system. Pheochromocytomas arise from paraganglia in the adrenal medulla whereas paragangliomas arise from extra-adrenal paraganglia. Sympathetic paraganglia are symmetrically distributed along the paravertebral axis from the superior cervical ganglion to the pelvis (46). Parasympathetic paraganglia serve as chemoreceptors and are located primarily in the head and neck and include the carotid and aortic bodies. The carotid bodies are located bilaterally at the carotid bifurcation while the aortic bodies are found along the aortic arch and at the aorticopulmonary region. Carotid body tumors are the most common paragangliomas of the head and neck (47) (Fig 7A). Other examples of head and neck paragangliomas include glomus jugulare, glomus tympanicum, and glomus vagale tumors.

Diagnosis of paraganglioma usually results from one of the following: (1) Signs/symptoms related to catecholamine hypersecretion (which can include hypertension, headaches, diaphoresis, palpitations, pallor and orthostasis), (2) symptoms related to mass effect on adjacent structures, (3) incidental radiologic detection, or (4) family screening for hereditary paraganglioma (46).

Intrathoracic paragangliomas account for <10% of all paragangliomas and clinically significant intrathoracic paragangliomas are found most commonly in the mediastinum (48). Paragangliomas can also be found in the lungs, trachea, heart, pericardium, and esophagus (49). Anterior and middle mediastinal paragangliomas (Fig 7B) usually arise from aortic body chemoreceptors at the aorticopulmonary region whereas posterior mediastinal paragangliomas (Fig 7C) arise from the paravertebral sympathetic chain (47). In terms of clinical features associated with mediastinal paragangliomas, 48% (15/31) of patients with paravertebral (i.e., posterior mediastinal) paragangliomas in one review (50) had symptoms related to

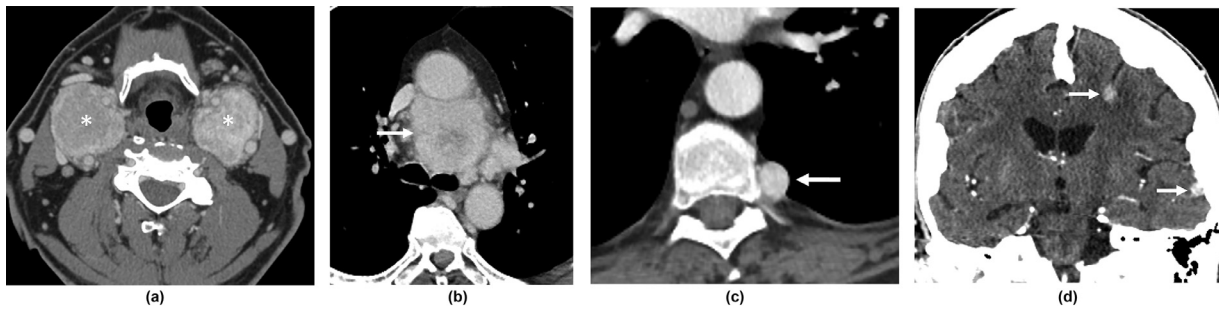


Figure 7. Paragangliomas.

A and B, A 67-year-old man with paraganglioma syndrome type 1. A, Contrast-enhanced neck CT performed for a tractor accident shows bilateral carotid body tumors (*asterisks*). B, Contrast-enhanced chest CT shows an avidly enhancing mediastinal mass (*arrow*), biopsy proven paraganglioma.

C, A 61-year-old woman undergoing family screening for familial paraganglioma syndrome. Contrast-enhanced chest CT shows an enhancing 1.5 cm left paravertebral nodule (*arrow*), biopsy proven paraganglioma. Genetic testing revealed familial paraganglioma syndrome type 4. Mediastinal paragangliomas typically occur near the aorticopulmonary window or paravertebral regions.

D, A 75-year-old woman with glomus vagale paraganglioma, metastatic to brain. Contrast-enhanced brain CT (coronal reformation) shows 2 enhancing metastatic lesions in the left cerebral hemisphere (*arrows*). More common causes of hypervascular metastases include lung, breast, renal, and thyroid malignancies as well as melanoma.

catecholamine hypersecretion, however, in another review (51), only 17% (2/12) of patients with posterior mediastinal paragangliomas had functional symptoms. Anterior and middle mediastinal paragangliomas likely have a lower incidence of functionality than posterior mediastinal paragangliomas (51) and are often detected incidentally (47).

Paragangliomas are usually sporadic but up to 10-50% are associated with inherited syndromes such as familial paraganglioma, neurofibromatosis type 1 (NF1), von Hippel-Lindau (VHL), and multiple endocrine neoplasia (MEN) Type 2 (46). Paragangliomas also occur as part of Carney's triad, comprised of paraganglioma, gastrointestinal stromal tumor (GIST) and pulmonary chondroma (46). Multicentric paragangliomas are well documented, especially with inherited syndromes. It is important to differentiate multicentric disease from metastatic disease; metastases occur in sites such as liver, lung, bone, and brain where there are no paraganglia (51) (Fig 7D).

When a catecholamine-secreting tumor is suspected clinically, biochemical documentation of catecholamine hypersecretion precedes imaging (46). Paragangliomas characteristically show intense homogeneous contrast enhancement on CT though larger tumors may show areas of low attenuation related to cystic degeneration or hemorrhage. Functional imaging with ^{123}I or ^{131}I metaiodobenzylguanidine (MIBG), ^{111}In -diethylenetriaminepentaacetic acid (DTPA)-pentetreotide (octreotide), and positron emission tomography (PET) are well-established modalities used to confirm diagnosis, identify disease sites, and evaluate for metastases (52). Conventional PET imaging using ^{18}F fluorodeoxyglucose (FDG) is highly sensitive in the detection of paraganglioma. The use of PET has increased with the development of newer radiotracers, for example, the ^{68}Ga -labeled somatostatin analogs, which improve the sensitivity and specificity of neuroendocrine tumor detection.

MENINGIOMAS

Meningiomas are a group of mostly benign and usually slow-growing tumors that are thought to originate from the meningotheial cells of the arachnoid layer (53). They are the most common primary tumor of the CNS, accounting for 37% of such tumors (54), and are often detected incidentally. Incidence increases with age, especially after age 65 (54). Meningiomas occur more commonly in females (53). Symptoms, when present, can be the result of compression of adjacent structures, invasion of or reactive changes in the adjacent brain, or obstruction of cerebrospinal fluid pathways, cortical veins, or venous sinuses (55). Meningiomas are classified as grade I (benign), II (atypical), or III (malignant) by the WHO (55). The majority (~80) is benign/grade I (54). The diagnosis of atypical/grade II meningioma (~18% of cases) requires specific histological features, however, brain invasion denotes at least a grade II tumor (56). Rates of recurrence are higher with grade II tumors (29-40%) (Fig 8A) than grade I tumors (7-20%) (55). Malignant/grade III meningiomas (~2% of cases) show a high frequency of local and brain invasion and recurrence (55). Extracranial metastases occur most often in association with WHO grade III tumors (53); metastatic sites can include the lungs, pleura, liver, and bone (Fig 8B). On CT, meningiomas are usually homogeneous, hyperdense, and classically associated with calcification; they typically enhance homogeneously (57). On MRI, they are usually isointense or slightly hypointense to cortex on T1-weighted imaging and hyperintense on T2-weighted imaging; post-contrast imaging shows a dural tail in 72% of cases (57). Features associated with atypical/malignant meningiomas include irregular margins, heterogeneity of tumor and enhancement pattern, significant peritumoral edema, necrosis, and bone destruction. However, these findings are not unique to higher grade tumors (57,58).

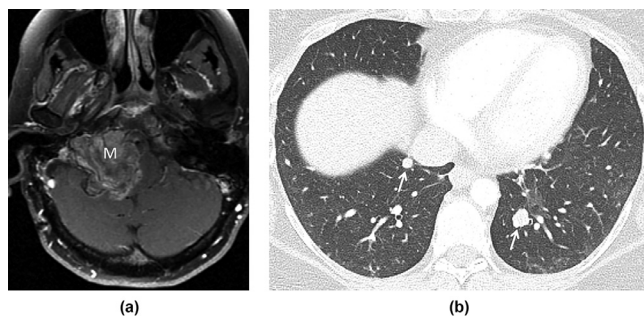


Figure 8. Meningioma.

A 37-year-old woman with recurrent atypical meningioma (WHO grade II), metastatic to lungs.

A, Axial contrast-enhanced T1-weighted MRI reveals the recurrent meningioma (M) at the right jugular foramen.

B, Contrast-enhanced chest CT (lung windows) performed 5 months later shows increase in size of metastatic pulmonary nodules (arrows) from atypical meningioma. Extracranial metastases occur most often in association with WHO grade III meningiomas; metastatic sites can include the lungs, liver, and bone.

MYASTHENIA GRAVIS AND THYMIC ABNORMALITIES

Myasthenia gravis (MG) is an autoimmune disorder characterized by weakness and fatigability of skeletal muscles. Muscle weakness can be generalized or localized, is more proximal than distal, and invariably affects the eye muscles, resulting in diplopia and ptosis (59). MG is usually mediated by autoantibodies against the acetylcholine receptor (AChR) and the thymus has a key role in inducing these autoantibodies in MG patients (59). Around 10% of patients with MG have thymoma, and the prevalence increases with increasing age, and MG occurs in 1/3 of patients with thymoma (59). Thymic hyperplasia is common in early-onset MG (i.e., onset before age 50) (59). MG patients with thymoma benefit from thymectomy (Fig 9); an even greater benefit from thymectomy has been reported for patients with early-onset MG without thymoma (59). A multicenter randomized trial of thymectomy and prednisone versus prednisone alone in nonthymomatous MG patients showed that thymectomy improved clinical outcomes (i.e., significant reductions in symptoms, immunosuppressive drug treatment, and exacerbations) over a 3-year period (60). Thymic hyperplasia tends to manifest with diffuse, symmetric enlargement of the thymus though atypical appearances (e.g., nodular or bulky configuration) can occur (61). Thymomas tend to be homogeneous or slightly heterogeneous with lobular contour (61).

VASCULAR

Vasculitis

The vasculitides are conditions that are characterized by inflammation of blood vessel walls. Vessel wall inflammation occurring at least at some point during the disease course is a shared

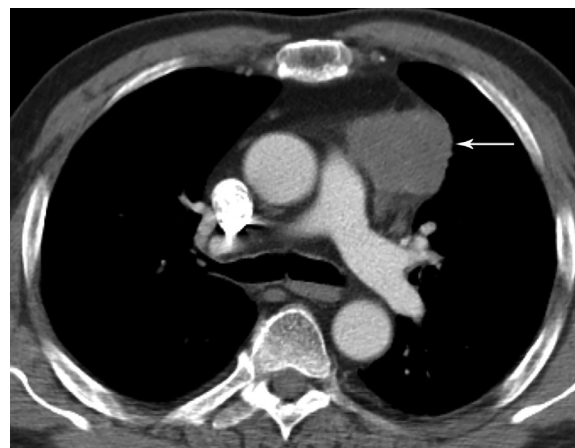


Figure 9. Thymoma and myasthenia gravis.

A 72-year-old man with myasthenia gravis (MG) and worsening fatigue with repetitive muscle use. Contrast-enhanced chest CT shows a smoothly margined solid anterior mediastinal mass (arrow), biopsy proven thymoma. Symptoms improved following resection. MG patients with thymoma often have reduction in symptoms after thymectomy and therefore thymectomy is indicated in all MG patients with thymoma.

defining feature of all vasculitides (62). Vasculitides may be broadly classified as infectious (i.e., known to be caused by direct invasion and proliferation of pathogens in vessel walls) or noninfectious (i.e., not known to be caused by direct vessel wall invasion by pathogens) (62). The noninfectious vasculitides are subdivided into large-, medium-, and small-vessel vasculitis based on the predominant type of vessels involved. It is important to note that vasculitis of all three major categories can affect any size artery (62). Large vessels include the aorta and its major branches and the venae cavae and their analogous veins. Medium vessels include the main visceral arteries and veins (e.g., coronary, mesenteric, hepatic, renal) and their initial branches. Small vessels include intraparenchymal arteries, arterioles, capillaries, venules, and veins (62). Clinical manifestations of the vasculitides are often vague and nonspecific and can include pain, fever, and elevated acute phase reactants. The following discussion will focus on the two major variants of large vessel vasculitis (LVV), i.e., giant cell arteritis (GCA) and Takayasu arteritis (TAK), both of which can have thoracic and neurologic manifestations.

GCA, the most common LVV in North America, is a disease of older individuals (age >50) and its prevalence rises with increasing age (63). GCA has a predilection for branches of the carotid and vertebral arteries and often involves the temporal artery (62,64) (Fig 10A). TAK affects younger individuals (age < 50), usually Asians, and predominantly affects the aorta and its major branches (Fig 10B). Both vasculitides are more common in women with female:male ratios of 3:1 and 8:1 respectively for GCA and TAK (64).

Owing to their sites of preferential involvement, neurologic symptoms are more common in GCA than in TAK (64). Up to 90% of GCA patients have neurologic symptoms of which headache is most common (64). Other

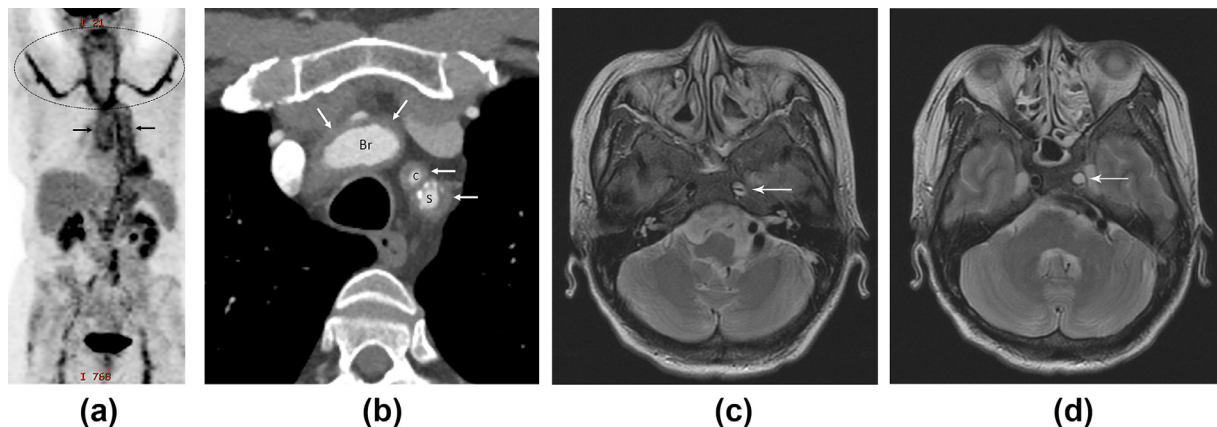


Figure 10. Large vessel vasculitides (LVVs).

A, A 74-year-old woman with fatigue, headache, and jaw claudication. Whole body PET shows markedly increased FDG uptake in the walls of aorta (*arrows*) and great vessels (*dashed oval*). Temporal artery biopsy revealed giant cell arteritis (GCA).

B, A 47-year-old man with Takayasu arteritis (TAK). The patient was diagnosed at the age of 37. Contrast-enhanced chest CT shows concentric wall thickening (*arrows*) of the great vessels. (Br = brachiocephalic artery, C = left common carotid artery, S = left subclavian artery). The characteristic feature of the LVVs (GCA and TAK) is concentric wall thickening of the aorta and/or great vessels. Neurologic manifestations are more common in GCA and include headache and stroke.

C and D, A 43-year-old Asian woman with Takayasu arteritis (TAK). Contrast-enhanced brain MRI shows an intimal flap in the left petrous carotid artery consistent with dissection (*arrow in C*) and abnormal signal intensity in the left carotid artery (*arrow in D*). (Color version of figure is available online.)

common symptoms include scalp tenderness, jaw claudication, and visual disturbances (as a result of temporal and occipital artery involvement). Irreversible blindness occurs in 20% of untreated cases and stroke occurs in ~7% (64). Constitutional symptoms are more commonly associated with TAK. TAK patients often present with limb claudication, bruits, absent/diminished/asymmetric pulses, asymmetric blood pressure measurements, and hypertension (64). Neurologic manifestations (e.g., light headedness, syncope, headache, visual impairment, stroke) occur in only ~1/3 of TAK patients and are typically late manifestations of the disease (64).

In terms of thoracic involvement, the characteristic feature of the LVVs is concentric wall thickening of the aorta and/or great vessels (63,65). Other findings associated with the LVVs include arterial stenosis and occlusion (Figs 10C and D). Less commonly, aneurysmal dilatation can occur after the medial layer is destroyed by inflammation (63). Chronic inflammation can lead to dystrophic calcification, which, in the case of TAK, is characteristically linear and occurs in the arch and descending thoracic aorta, sparing the ascending aorta (65). PET/CT can be used to confirm the presence of vascular inflammation when clinical and other imaging findings are nonspecific (66).

HEREDITARY CONDITIONS

Hereditary Hemorrhagic Telangiectasia

Hereditary hemorrhagic telangiectasia (HHT), known also as Osler-Weber-Rendu disease, is an autosomal dominant disorder most commonly caused by mutations in *ENG*

(encoding for endoglin) (HHT type 1) or *ACVRL1* (encoding for activin receptor-like kinase 1) (HHT type 2) (67). The *ENG* and *ACVRL1* genes code for proteins that are involved in normal blood vessel development (67). HHT is characterized by spontaneous and recurrent epistaxis, multiple mucocutaneous telangiectasias at characteristic sites (lips, oral cavity, fingers, nose), and visceral lesions (e.g., gastrointestinal telangiectasia or pulmonary, cerebral, spinal, or hepatic arteriovenous malformations [AVMs]) (68). Manifestations of HHT are not generally present at birth; childhood epistaxis is usually the earliest sign (69). Pulmonary AVMs (PAVMs) often become apparent after puberty and mucocutaneous and GI telangiectasias develop with increasing age (69). PAVMs are capillary-free communications between the pulmonary and systemic circulations (i.e., right-to-left shunts) comprised of (1) one or more feeding artery/arteries, (2) an aneurysmal sac or serpiginous network, and (3) one or more draining vein[s] (67,70) (Fig 11A). Clinical presentations of PAVMs include: (1) paradoxical embolism (i.e., venous embolic material reaches the arterial circulation), which may lead to severe neurologic complications such as stroke, transient ischemic attack, or cerebral abscess (Fig 11B), (2) spontaneous rupture (a relatively rare feature), leading to hemoptysis or hemothorax, and (3) dyspnea and asymptomatic hypoxemia (69,70). Prevalence of PAVMs varies by genotype; one series showed PAVMs on CT in 58% with HHT1 and 18% with HHT2 (71). CT is the modality of choice for diagnosis and evaluation of PAVMs (70). PAVMs have a predilection for the lower lobes and are often multiple in HHT patients (72). Treatment is by transcatheter embolotherapy; selection for embolization is based on feeding artery diameter (≥ 3 mm, though smaller diameter lesions may be targeted) (73). A

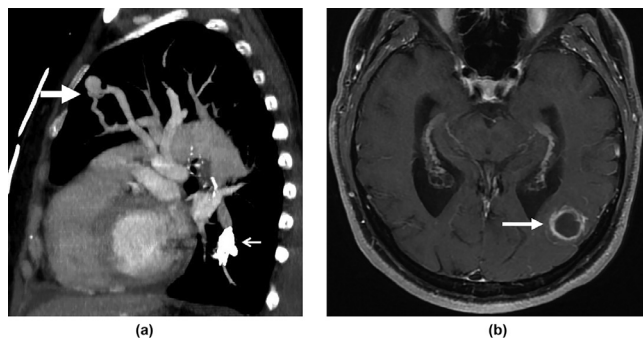


Figure 11. Hereditary hemorrhagic telangiectasia (HHT). A, A 55-year-old woman with HHT. Contrast-enhanced sagittal maximum intensity projection (MIP) image shows a pulmonary arteriovenous malformation (PAVM, large arrow) in the left upper lobe. Note also metallic density in the left lower lobe (small arrow) related to coil embolization of a different PAVM.

B, A 60-year-old man with cerebral abscess. T1-weighted contrast-enhanced brain MRI shows a left parietal rim-enhancing lesion consistent with abscess (arrow). PAVMs are right-to-left shunts and can lead to paradoxical emboli, resulting in stroke or intracranial abscess.

variety of cerebral vascular malformations (CVMs) can occur in HHT, most commonly cerebral AVMs (CAVMs), arteriovenous fistulae (AVFs), microAVMs (<1 cm) and telangiectasias (73). Approximately 23% of HHT patients will have a CVM and bleeding risk has been estimated at ~0.5%/year (73). Due to the risk of life-threatening complications, all patients with HHT are screened for PAVMs and CAVMs (73).

Tuberous Sclerosis Complex

Tuberous sclerosis complex (TSC) is an autosomal dominant syndrome characterized by the development of benign hamartomas in multiple organs including the brain, eyes,

heart, lungs, liver, kidney, and skin. TSC results from mutations in the tumor suppressor genes *TSC1* and *TSC2*(74). Diagnosis is based on genetic testing and/or clinical findings (75). Most features of TSC become evident only after the age of 3 (76). CNS abnormalities result in the greatest morbidity and mortality in TSC and include cortical dysplasias, subependymal nodules, and subependymal giant cell astrocytomas (75) (Fig 12A). Pulmonary features of TSC include cysts in lymphangioliomyomatosis (LAM) and nodules in multifocal micronodular pneumocyte hyperplasia (MMPH) (75). Found in 30–40% of female TSC patients, LAM is the primary pulmonary manifestation of TSC and manifests as thin-walled cysts evenly distributed throughout the lungs (75) (Fig 12B). Patients with LAM typically present with progressive dyspnea on exertion and recurrent pneumothoraces in the third to fourth decade (75). MMPH results from proliferation of type II alveolar cells and manifests on CT with nodules ranging from 1 to 10 mm in size (74) (Fig 12C). Cardiac rhabdomyomas are highly specific for TSC and may be the first manifestation of the disease. Cardiac rhabdomyomas are often observed in the fetus and can regress after birth (75).

Neurofibromatosis Type 1

Neurofibromatosis type 1 (NF1) is an autosomal dominant disorder that results from a mutation in the *NF1* tumor-suppressor gene (77). The hallmark of NF1 is neurofibromas, benign tumors arising from peripheral nerves. However, there are multiple other tumoral (both benign and malignant) and nontumoral manifestations of NF1 (78). In fact, hyperpigmented café-au-lait macules, which usually develop by age 2, are frequently the earliest clinical manifestation (77). In the thorax, neurofibromas may arise in the skin and subcutaneous soft tissues or from the sympathetic chain, intercostal, phrenic, or vagus nerves (Fig 13A). On CT, neurofibromas tend to be homogeneous, smoothly margined, and rounded or elliptical in morphology. On MRI, they show low to

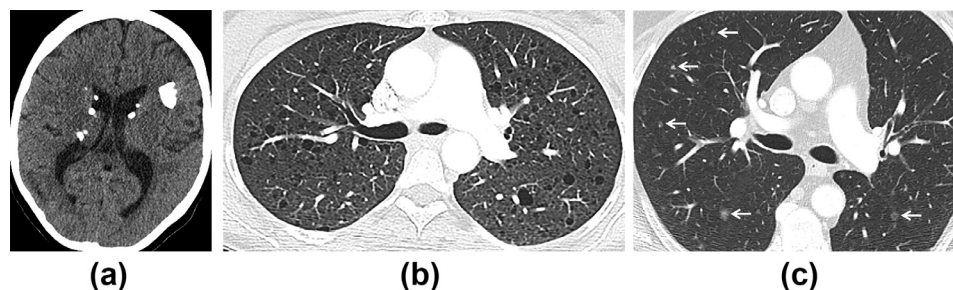


Figure 12. Tuberous sclerosis complex (TSC).

A, A 20-year-old woman. Noncontrast CT brain shows multiple calcified subependymal nodules along the lateral ventricles and a large calcified cortical tuber (a type of focal cortical dysplasia) in the left frontal lobe. CNS abnormalities in TSC include cortical dysplasias, subependymal nodules, and subependymal giant cell astrocytomas.

B, A 42-year-old woman. Contrast-enhanced chest CT (lung windows) shows diffuse distribution of thin-walled cysts consistent with TSC-related lymphangioliomyomatosis (LAM).

C, A 54-year-old man. Contrast-enhanced chest CT (lung windows) shows numerous small ground-glass and solid lung nodules (arrows), consistent with multifocal micronodular pneumocyte hyperplasia (MMPH). Lung manifestations in TSC patients include cysts (LAM) and nodules (MMPH).

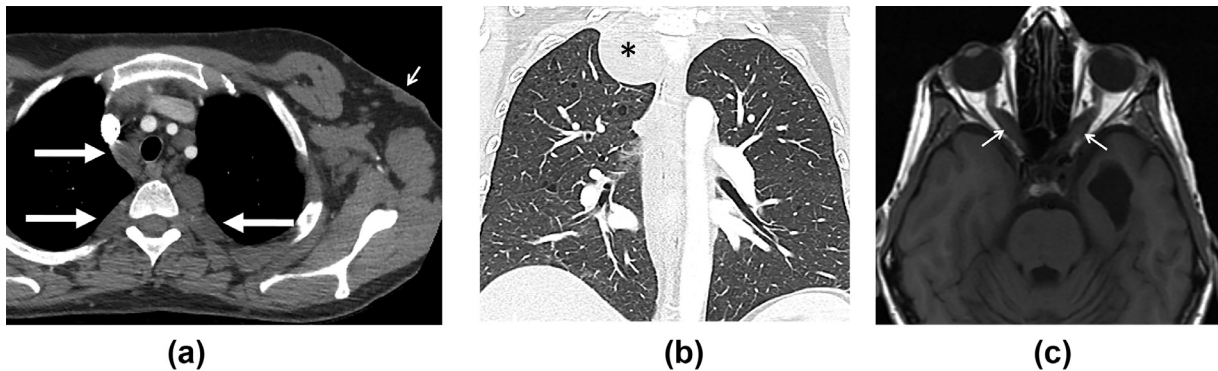


Figure 13. Neurofibromatosis type 1 (NF1).

A, A 29-year-old man. Contrast-enhanced chest CT shows mediastinal and paravertebral neurofibromas (long arrows). Note left axillary cutaneous neurofibroma (short arrow).

B, A 36-year-old woman. Contrast-enhanced coronal CT reformation shows upper lobe predominant lung cysts and a right apical/paravertebral neurofibroma (*).

C, A 28-year-old man. Non-contrast T1-weighted MRI shows bilateral optic nerve gliomas (arrows). Around 15%-20% of NF1 patients develop low-grade glial neoplasms, most of which involve the optic pathway.

intermediate in signal intensity on T1-weighted images and high signal intensity (often heterogeneous) on T2-weighted images with high signal regions corresponding to areas of myxoid tissue or cystic degeneration (79). Other intrathoracic manifestations of NF1 include lateral meningoceles and skeletal abnormalities such as kyphoscoliosis, rib erosions and deformities, and vertebral scalloping. Pulmonary involvement is reported in a minority of adults with NF1 and is characterized by upper lobe predominant cystic (Fig 13B) and bullous disease and lower lobe fibrosis (80–82). Upper lobe centrilobular ground-glass nodules may be seen (82). In terms of the CNS, 15–20% of patients develop low-grade glial neoplasms, of which 80% involve the optic pathway (77) (Fig 13C). Optic pathway gliomas can be asymptomatic; when symptomatic, reduced vision is most common (77).

CONCLUSION

A wide variety of conditions can affect both the neurological system and the thorax. Knowledge of these entities allows the radiologist to do a targeted search for pertinent clinical manifestations in the patients' history and correlate with radiologic findings on relevant imaging studies. Correlation of signs, symptoms, and imaging findings in the neurological system with those in the thorax are integral to diagnose these conditions and/or guide further diagnostic work-up and treatment.

REFERENCES

- Umehara H, Okazaki K, Masaki Y, et al. Comprehensive diagnostic criteria for IgG4-related disease (IgG4-RD). *Mod Rheumatol* 2011; 22:21–30.
- Stone JH, Zen Y, Deshpande V. IgG4-related disease. *N Engl J Med* 2012; 366:539–551.
- Martinez-de-Alegria A, Baleato-González S, García-Figueiras R, et al. IgG4-related Disease from Head to Toe. *Radiographics* 2015; 35:2007–2025.
- Fei Y, Shi J, Lin W, et al. Intrathoracic involvements of immunoglobulin g4-related sclerosing disease. *Medicine* 2015; 94:e2150.
- Inoue D, Zen Y, Abo H, et al. Immunoglobulin G4-related lung disease: CT findings with pathologic correlations. *Radiology* 2009; 251:260–270.
- Oyama-Manabe N, Yabusaki S, Manabe O, Kato F, Kanno-Okada H, Kudo K. IgG4-related Cardiovascular Disease from the Aorta to the Coronary Arteries: Multidetector CT and PET/CT. *Radiographics* 2018; 38:1934–1948.
- Yabusaki S, Oyama-Manabe N, Manabe O, et al. Characteristics of immunoglobulin G4-related aortitis/peri-aortitis and periarteritis on fluoro-deoxyglucose positron emission tomography/computed tomography co-registered with contrast-enhanced computed tomography. *EJNMMI Res* 2017; 7:20.
- AbdelRazek MA, Venna N, Stone JH. IgG4-related disease of the central and peripheral nervous systems. *Lancet Neurol* 2018; 17:183–192.
- Kashii S. IgG4-related disease: a neuro-ophthalmological perspective. *J Neuroophthalmol* 2014; 34:400–407.
- Baptista B, Casian A, Gunawardena H, D'Cruz D, Rice CM. Neurological manifestations of igg4-related disease. *Curr Treat Options Neurol* 2017; 19:14.
- Wallace ZS, Zhang Y, Perugini CA, Naden R, Choi HK, Stone JH. ACR/EULAR IgG4-RD Classification Criteria Committee. Clinical phenotypes of IgG4-related disease: an analysis of two international cross-sectional cohorts. *Ann Rheum Dis* 2019; 78:406–412.
- Dalakas MC, Hohlfield R. Polymyositis and dermatomyositis. *Lancet* 2003; 362:971–982.
- Douglas WW, Tazelaar HD, Hartman TE, et al. Polymyositis-dermatomyositis-associated interstitial lung disease. *Am J Respir Crit Care Med* 2001; 164:1182–1185.
- Hill CL, Zhang Y, Sigurgeirsson B, et al. Frequency of specific cancer types in dermatomyositis and polymyositis: a population-based study. *Lancet* 2001; 357:96–100.
- Selva-O'Callaghan A, Grau JM, Gámez-Cenzano C, et al. Conventional cancer screening versus PET/CT in dermatomyositis/polymyositis. *Am J Med* 2010; 123:558–562.
- Sandhu NP, Zakaria S, Degnim AC, Boughey JC. Dermatomyositis presenting as a paraneoplastic syndrome due to underlying breast cancer. *BMJ Case Rep* 2011 Feb 2: 2011.
- Iannuzzi MC, Rybicki BA, Teirstein AS. Sarcoidosis. *N Engl J Med* 2007; 357:2153–2165.
- Nowak DA, Widenka DC. Neurosarcoidosis: a review of its intracranial manifestation. *J Neurol* 2001; 248:363–372.
- Lury KM, Smith JK, Matheus MG, Castillo M. Neurosarcoidosis—review of imaging findings. *Semin Roentgenol* 2004; 39:495–504.
- World Health Organization website. <https://www.who.int/news-room/detail/27-04-2020-who-timeline-covid-19> Accessed May 11, 2020.
- Hopkins Johns. <https://coronavirus.jhu.edu/map.html> Accessed May 19, 2020.
- Wang D, Hu B, Hu C, et al. Clinical characteristics of 138 hospitalized patients with 2019 novel coronavirus-infected pneumonia in wuhan. *China. JAMA* 2020. doi:10.1001/jama.2020.1585. [Epub ahead of print].

23. Chung M, Bernheim A, Mei X, et al. CT Imaging Features of 2019 Novel Coronavirus (2019-nCoV). *Radiology* 2020; 295:202–207.
24. Salehi S, Abedi A, Balakrishnan S, Gholamrezanezhad A. Coronavirus disease 2019 (COVID-19): a systematic review of imaging findings in 919 patients. *AJR Am J Roentgenol* 2020; 1–7. doi:10.2214/AJR.20.23034. [Epub ahead of print].
25. Simpson S, Kay FU, Abbara S, et al. Radiological Society of North America Expert Consensus Statement on Reporting Chest CT Findings Related to COVID-19. Endorsed by the Society of Thoracic Radiology, the American College of Radiology, and RSNA. *J Thorac Imaging* 2020. doi:10.1097/RTI.0000000000000524. [Epub ahead of print].
26. Liang T, Liu Z, Wu CC, et al. Evolution of CT findings in patients with mild COVID-19 pneumonia. *Eur Radiol* 2020. doi:10.1007/s00330-020-06823-8. [Epub ahead of print].
27. Zhou S, Wang Y, Zhu T, Xia L. CT Features of Coronavirus Disease 2019 (COVID-19) Pneumonia in 62 Patients in Wuhan. China. *AJR Am J Roentgenol* 2020 Mar 5; 1–8. doi:10.2214/AJR.20.22975. [Epub ahead of print].
28. Bernheim A, Mei X, Huang M, et al. Chest CT Findings in Coronavirus Disease-19 (COVID-19): Relationship to Duration of Infection. *Radiology* 2020 Feb 20:200463 doi:10.1148/radiol.2020200463. [Epub ahead of print].
29. Mao L, Jin H, Wang M, et al. Neurologic Manifestations of Hospitalized Patients With Coronavirus Disease 2019 in Wuhan. China. *JAMA Neurol* 2020 Apr 10. doi:10.1001/jamaneurol.2020.1127. [Epub ahead of print].
30. Oxley TJ, Mocco J, Majidi S, et al. Large-Vessel Stroke as a Presenting Feature of Covid-19 in the Young. *N Engl J Med* 2020 Apr 28. doi:10.1056/NEJMc2009787. [Epub ahead of print].
31. Helms J, Kremer S, Merdji H, et al. Neurologic features in severe sars-cov-2 infection. *N Engl J Med* 2020 Apr 15. doi:10.1056/NEJMc2008597. [Epub ahead of print].
32. Filatov A, Sharma P, Hindi F, Espinosa PS. Neurological Complications of Coronavirus Disease (COVID-19): Encephalopathy. *Cureus* 2020; 12: e7352.
33. Poyiadji N, Shahin G, Noujaim D, Stone M, Patel S, Griffith B. COVID-19-associated Acute Hemorrhagic Necrotizing Encephalopathy: CT and MRI Features. *Radiology* 2020 Mar 31:201187. doi:10.1148/radiol.2020201187. [Epub ahead of print].
34. Toscano G, Palmerini F, Ravaglia S, et al. Guillain-Barré Syndrome Associated with SARS-CoV-2. *N Engl J Med* 2020 Apr 17. doi:10.1056/NEJMc2009191. [Epub ahead of print].
35. Segal BH. Aspergillosis. *N Engl J Med* 2009; 360:1870–1884.
36. Franquet T, Gimenez A, Hidalgo A. Imaging of opportunistic fungal infections in immunocompromised patient. *European journal of radiology* 2004; 51:130–138.
37. Caillot D, Couaillier JF, Bernard A, et al. Increasing volume and changing characteristics of invasive pulmonary aspergillosis on sequential thoracic computed tomography scans in patients with neutropenia. *J Clin Oncol* 2001; 19:253–259.
38. Brodoefel H, Vogel M, Hebart H, et al. Long-term CT follow-up in 40 non-HIV immunocompromised patients with invasive pulmonary aspergillosis: kinetics of CT morphology and correlation with clinical findings and outcome. *AJR Am J Roentgenol* 2006; 187:404–413.
39. Raviglione MC. Tuberculosis. In: Jameson J, Fauci AS, Kasper DL, Hauser SL, Longo DL, Loscalzo J, eds. *Harrison's Principles of Internal Medicine*, 20e, New York, NY: McGraw-Hill; 2018 <http://accessmedicine.mhmedical.com/content.aspx?bookid=2129§ionid=192023354>.
40. Marais BJ, Parker SK, Verver S, van Rie A, Warren RM. Primary and post-primary or reactivation tuberculosis: time to revise confusing terminology? *AJR Am J Roentgenol* 2009; 192:W198. author reply W199–200.
41. Nachiappan AC, Rahbar K, Shi X, et al. Pulmonary Tuberculosis: Role of Radiology in Diagnosis and Management. *Radiographics* 2017; 37:52–72.
42. van Rie A, Warren R, Richardson M, et al. Exogenous reinfection as a cause of recurrent tuberculosis after curative treatment. *N Engl J Med* 1999; 341:1174–1179.
43. Jeong YJ, Lee KS. Pulmonary tuberculosis: up-to-date imaging and management. *AJR Am J Roentgenol* 2008; 191:834–844.
44. Lichtenberger JP 3rd, Sharma A, Zachary KC, et al. What a differential a virus makes: a practical approach to thoracic imaging findings in the context of HIV infection—part 1, pulmonary findings. *AJR Am J Roentgenol* 2012; 198:1295–1304.
45. Burrill J, Williams CJ, Bain G, Conder G, Hine AL, Misra RR. Tuberculosis: a radiologic review. *Radiographics* 2007; 27:1255–1273.
46. Young WF Jr. Paragangliomas: clinical overview. *Ann N Y Acad Sci* 2006; 1073:21–29.
47. Lee KY, Oh YW, Noh HJ, et al. Extraadrenal paragangliomas of the body: imaging features. *AJR Am J Roentgenol* 2006; 187:492–504.
48. Erickson D, Kudva YC, Ebersold MJ, et al. Benign paragangliomas: clinical presentation and treatment outcomes in 236 patients. *J Clin Endocrinol Metab* 2001; 86:5210–5216.
49. Ocazionez D, Shroff GS, Vargas D, et al. Imaging of Intrathoracic Paragangliomas. *Semin Ultrasound CT MR* 2017; 38:584–593.
50. Gallivan MV, Chun B, Rowden G, Lack EE. Intrathoracic paravertebral malignant paraganglioma. *Arch Pathol Lab Med* 1980; 104:46–51.
51. Moran CA, Suster S, Fishback N, Koss MN. Mediastinal paragangliomas. A clinicopathologic and immunohistochemical study of 16 cases. *Cancer* 1993; 72:2358–2364.
52. Baez JC, Jagannathan JP, Krajewski K, et al. Pheochromocytoma and paraganglioma: imaging characteristics. *Cancer Imaging* 2012; 12:153–162.
53. Perry A, Louis DN, Budka H, et al. Meningiomas. In: Louis DN, ed. *WHO Classification of Tumours of the Central Nervous System Revised fourth edition*, Lyon: International Agency For Research On Cancer; 2016:232–245.
54. Ostrom QT, Gittleman H, Truitt G, Boscia A, Kruchko C, Barnholtz-Sloan JS. *CBTRUS Statistical Report: Primary Brain and Other Central Nervous System Tumors Diagnosed in the United States in 2011–2015*. *Neuro Oncol* 2018; 20:iv1–iv86.
55. Whittle IR, Smith C, Navoo P, Collie D. Meningiomas. *Lancet* 2004; 363:1535–1543.
56. Louis DN, Perry A, Reifenberger G, et al. The 2016 World Health Organization Classification of Tumors of the Central Nervous System: a summary. *Acta Neuropathol* 2016 Jun; 131:803–820.
57. Huang RY, Bi WL, Griffith B, et al. Imaging and diagnostic advances for intracranial meningiomas. *Neuro Oncol* 2019; 21(Suppl 1):i44–i61.
58. Kunimatsu A, Kunimatsu N, Kamiya K, Katsura M, Mori H, Ohtomo K. Variants of meningiomas: a review of imaging findings and clinical features. *Jpn J Radiol* 2016; 34:459–469.
59. Gilhus NE. Myasthenia Gravis. *N Engl J Med* 2016; 375:2570–2581.
60. Wolfe GI, Kaminski HJ, Aban IB, et al. Randomized Trial of Thymectomy in Myasthenia Gravis. *N Engl J Med* 2016; 375:511–522.
61. Carter BW, Okumura M, Detterbeck FC, Marom EM. Approaching the patient with an anterior mediastinal mass: a guide for radiologists. *J Thorac Oncol* 2014; 9(9 Suppl 2):S110–S118.
62. Jennette JC, Falk RJ, Bacon PA, et al. 2012 revised International Chapel Hill Consensus Conference Nomenclature of Vasculitides. *Arthritis Rheum* 2013; 65:1–11.
63. Restrepo CS, Ocazionez D, Suri R, Vargas D. Aortitis: imaging spectrum of the infectious and inflammatory conditions of the aorta. *Radiographics* 2011; 31:435–451.
64. Ponte C, Águeda AF, Luqmani RA. Clinical features and structured clinical evaluation of vasculitis. *Best Pract Res Clin Rheumatol* 2018; 32:31–51.
65. Matsunaga N, Hayashi K, Sakamoto I, Ogawa Y, Matsumoto T. Takayasu arteritis: protean radiologic manifestations and diagnosis. *Radiographics* 1997; 17:579–594.
66. Abdel Razek AA, Alvarez H, Bagg S, Refaat S, Castillo M. Imaging spectrum of CNS vasculitis. *Radiographics* 2014; 34:873–894.
67. Lacombe P, Lacout A, Marcy PY, et al. Diagnosis and treatment of pulmonary arteriovenous malformations in hereditary hemorrhagic telangiectasia: An overview. *Diagn Interv Imaging* 2013; 94:835–848.
68. Fuchizaki U, Miyamori H, Kitagawa S, Kaneko S, Kobayashi K. Hereditary haemorrhagic telangiectasia (Rendu-Osler-Weber disease). *Lancet* 2003; 362:1490–1494.
69. Begbie ME, Wallace GM, Shovlin CL. Hereditary haemorrhagic telangiectasia (Osler-Weber-Rendu syndrome): a view from the 21st century. *Postgrad Med J* 2003; 79:18–24.
70. Shovlin CL. Pulmonary arteriovenous malformations. *Am J Respir Crit Care Med* 2014; 190:1217–1228.
71. van Gent MW, Post MC, Snijder RJ, Westermann CJ, Plokker HW, Mager JJ. Real prevalence of pulmonary right-to-left shunt according to genotype in patients with hereditary hemorrhagic telangiectasia: a transthoracic contrast echocardiography study. *Chest* 2010; 138:833–839.
72. Jaskolka J, Wu L, Chan RP, Faughnan ME. Imaging of hereditary hemorrhagic telangiectasia. *AJR Am J Roentgenol* 2004; 183:307–314.
73. Faughnan ME, Palda VA, Garcia-Tsao G, et al. International guidelines for the diagnosis and management of hereditary haemorrhagic telangiectasia. *J Med Genet* 2011; 48:73–87.

74. Franz DN, Brody A, Meyer C, et al. Mutational and radiographic analysis of pulmonary disease consistent with lymphangioleiomyomatosis and micronodular pneumocyte hyperplasia in women with tuberous sclerosis. *Am J Respir Crit Care Med* 2001; 164:661–668.
75. Northrup H, Krueger DA. International Tuberous Sclerosis Complex Consensus Group. Tuberous sclerosis complex diagnostic criteria update: recommendations of the 2012 International Tuberous Sclerosis Complex Consensus Conference. *Pediatr Neurol* 2013; 49:243–254.
76. Curatolo P, Bombardieri R, Jozwiak S. Tuberous sclerosis. *Lancet* 2008; 372:657–668.
77. Hirbe AC, Gutmann DH. Neurofibromatosis type 1: a multidisciplinary approach to care. *Lancet Neurol* 2014; 13:834–843.
78. Korf BR. Neurofibromatosis. *Handb Clin Neurol* 2013; 111:333–340.
79. Fortman BJ, Kuszyk BS, Urban BA, Fishman EK. Neurofibromatosis type 1: a diagnostic mimicker at CT. *Radiographics* 2001; 21:601–612.
80. Zamora AC, Collard HR, Wolters PJ, Webb WR, King TE. Neurofibromatosis-associated lung disease: a case series and literature review. *Eur Respir J* 2007; 29:210–214.
81. Alves Júnior SF, Zanetti G, Alves de Melo AS. Neurofibromatosis type 1: State-of-the-art review with emphasis on pulmonary involvement. *Respir Med* 2019; 149:9–15.
82. Oikonomou A, Vadikolias K, Birbilis T, Bouros D, Prassopoulos P. HRCT findings in the lungs of non-smokers with neurofibromatosis. *Eur J Radiol* 2011; 80:e520–e523.